A Novel Design for Improving the Control on the Stainless-Steel Vessel Welding Process for Superconducting Magnets

G. Vallone, G. Ambrosio, E. Anderssen, S. Fehrer, P. Ferracin, J. Ferradas Troitino

***Abstract*—Stainless steel vessels see widespread use in superconducting magnets for particle accelerator applications. Their function varies in different magnet designs: they always provide the necessary liquid helium containment, but in some cases are also used to provide azimuthal prestress and can also be welded to the magnet end plate to provide additional longitudinal stiffness. A magnet designed with the bladder and key technology does not rely on the structural role of the vessel. They are structurally supported using azimuthally prestressed aluminum shells, and the longitudinal constraint by rods. In this case, the magnet designer would generally like to minimize the interaction between the magnet and the stainless-steel vessel and to minimize the coil stress variation due to the vessel. The stress state in the vessel and in the coil is a function of the circumferential interference, defined as the vessel azimuthal length minus the magnet circumference. The vessel and the magnet azimuthal length machining tolerances are relatively large resulting in significant stress variations in the superconducting coils. In this paper we introduce an interference-control shim, which can significantly limit the stress variation of the coils for a given variation of the interference. The effectiveness of the interference-control shim is evaluated numerically on the MQXF, the low-β quadrupole for the High Luminosity LHC.**

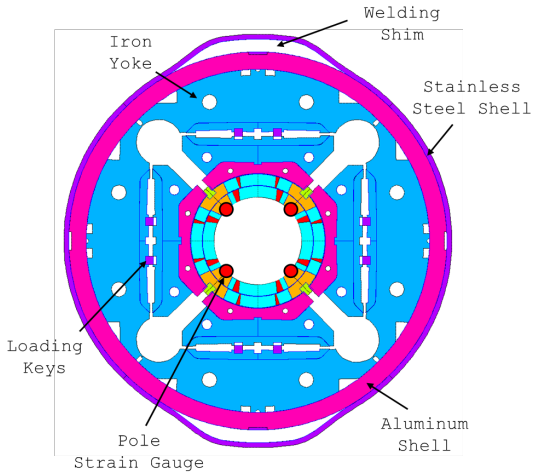

Fig. 1. Magnified deformation of the MQXF magnet after welding, with the welding shims installed on top and bottom.

I. Introduction

SUPERCONDUCTING magnets for particle accelerators have used a cold yoke ever since it was introduced in the Isabelle dipole magnets [1]. In general, the cold yoke is encased in stainless steel shells (vessel) that contain the helium. Often, the helium vessel also has a mechanical support function: this is the case, for example, in the RHIC, LHC and 11 T dipole magnet designs [2]–[4]. Depending on the design, the vessel can provide radial stiffness, for example bringing in contact the iron yoke halves, or also some prestress to the superconducting coils, in an attempt to avoid coil/pole separation during powering [5]. In other designs, as for example the HERA and SSC dipoles [6], [7], the vessel is limited to a helium containment function. This is also the case for modern bladder and key design [8] magnets, as for example MQXF [9], where the prestress is completely provided by an aluminum shell inside the cold mass.

When the mechanical support is not needed, it is desirable to limit or even completely remove the mechanical interaction between the stainless steel vessel and the magnet. The mechanical contact can in fact have harmful effects on the magnet performances, increasing the internal forces in the superconducting coils, which can eventually lead to their failure, or introducing undesired frictional interactions during the thermal cycles. Nevertheless, the friction between the vessel and the magnet can allow to control their relative position, in turn guaranteeing the position of the magnet within the cryostat.

Helium vessels are composed of two stainless steel half-shells, wrapped around the magnet and welded along the mid-plane. The amount of interaction (contact force) between the magnet and the vessel is governed by three parameters: the developed length of the magnet and of the vessel, and the shrinkage of the welds. Unfortunately, even small assembly tolerances can lead to a dangerous stress increase in the coils, often forcing the magnet designer to allow for a large gap between the vessel and the magnet. In this paper we introduce a novel concept that can improve the control of the vessel to magnet interaction, and then propose its application to the MQXFA magnet [10].

This work was supported by the High Luminosity LHC Project at CERN and by the DOE through the U.S. LHC Accelerator Research Program.

G. Vallone, E. Anderssen and P. Ferracin are with Lawrence Berkeley National Laboratory, Berkeley, CA 94720 USA (e-mail: gvallone@lbl.gov).

G. Ambrosio and S. Fehrer are with the Fermi National Accelerator Laboratory, Batavia, IL 80510 USA.

J. Ferradas Troitino is with the European Organization for Nuclear Research, Geneva, CH.

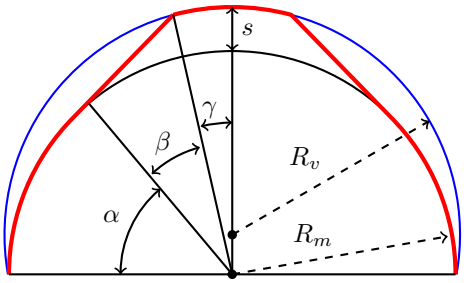

Fig. 2. Vessel welding with a welding shim of thickness s. γ is the angle where the vessel gets in contact with the magnet, and β the angle where the welding shim ends. The vessel is shown in blue, the magnet in black, and the final shape after welding in red.

II. The Welding Shim Concept

The vessel is composed of two stainless steel shells welded on the magnet mid-plane. If the developed length of the shells πR_v, minus the shrinkage of the welds w, is smaller than the magnet circumference $2\pi R_m$, the final configuration presents an interference. The total force stretching the vessel, in equilibrium with the compressive force in the magnet, can be computed as:

$$F_c = EA\varepsilon_\theta = EA\frac{\pi R_v - w - \pi R_m}{\pi R_v - w} \tag{1}$$

where ε_θ is the average azimuthal strain in the vessel, E the modulus, and A the cross-sectional area. This formula is valid if the dimensional change of the magnet due to the vessel force is negligible. $2\pi R_v - 2w - 2\pi R_m$ is the circumferential interference between the vessel and the magnet: the larger the interference, the larger will be the force exchanged between the vessel and the magnet and the increase in coil stress. With this welding strategy, as soon as the vessel is in contact with the magnet the force quickly increases: considering a typical vessel thickness is of 10 mm, a 0.1% error in the circumferential interference would generate a force of 2 MN/m, or on a 40 mm thick coil, an average stress of 50 MPa, with eventual higher peaks due to bending.

In order to decrease this sensitivity, here we propose to add a short steel welding shim on the two magnet sides, as shown in Fig. 1. The welding shim is installed on the magnet top and bottom side, and it creates a space where the vessel deforms but is still not completely in contact with the magnet. This intermediate region of contact can introduce a buffer region, where the vessel stress (and the contact force) increase, but the pole and coil stress do not. The length L_v of the vessel after getting in contact with the shim and the magnet, with reference to Fig. 2, can be approximated as:

$$L_{vs} = R_m(\pi - 2\beta - 2\gamma) + (R_m + s)(2\beta + 2\gamma) \tag{2}$$

where s is the thickness of the welding shim, R_m is the radius of the magnet, β is the angular length of the welding shim, and γ is the angular length of the bending region. If $\beta+\gamma$ is equal to $\pi/4$, the available deformation in the bending region is equal to:

$$\varepsilon_\theta = \frac{L_{vs} - \pi R_m}{\pi R_m} = \frac{s}{2R_m} \tag{3}$$

This means that, with a shim thickness of 1/100 times the magnet radius, we could introduce an intermediate region allowing for a 0.1% error in the circumferential length.

III. The MQXF magnet

The MQXF magnet is being developed as part of the High-Luminosity upgrade [11], in order to substitute the LHC inner triplet quadrupoles currently in use. The magnet, whose cross-section is shown in Fig. 1, targets a gradient of 132.2 T/m in a 150 mm aperture, when powered at 16.23 kA. The design employs the bladder and key technology to apply the azimuthal prestress to the coils [8]. The longitudinal prestress is realized with rods, stretched by a piston and locked in place with nuts and bolts. An important feature of the magnet design is that strain measurements on the winding pole (see Fig. 1) provides a good indication of the coil stress at all stages [12].

The original design aimed at using the stainless steel shell only for LHe containment, and a 3.2 MPa increase limit on the winding pole azimuthal stress was established. However, in a recent development it was decided to attempt and use the contact force between the vessel and the magnet to prevent relative motions. During its life cycle, the magnet can see unbalanced longitudinal loads only during transportation or in the case of a pressure wave due to a quench. The transportation load is equal to 135 kN, considering a load of about 10 g. The pressure wave is expected to be less than 2.5 bar. Considering the magnet cross-section, this is equal to a load of 61.8 kN on one side of the magnet. Given the strict limit on the coil stress variation due to the vessel welding, and the considerations from Section II, this would not be feasible with a traditional welding process. Thus the welding shim concept was introduced.

IV. Experimental Measurements

A. Tolerance Measurement

The final interference is a function of three quantities:

1) Vessel Developed Length: Controlling a 10 m long, 8 mm thick bump formed stainless steel half cylinder (shell) developed length is not easy, neither is measuring the obtained length. In order to have the best precision for machining, the shell is clamped to pre-machined forms. As long as the bump formed shell curvature is uniform, this method can give the best accuracy for the developed length. After machining the SS shells, their inner half circumference needs to be measured. The inner surface is measured with survey maps made with a laser tracker. Due to the imperfect shape of the inner surface, left by the bump forming method, the measurement and manufacturing precision are within half a millimeter.

2) Magnet Outer Circumference: The aluminium shells are machined with high precision to ensure prestress uniformity along the magnet length. However, after the prestress is applied, the ends of the shells are a bit larger than the middle of the cylinder. This variation is in the order of 0.1 - 0.2 mm, significantly smaller than the variation of the SS shell developed length.

3) Weld Shrinkage: 8 weld samples were made to determine the shrinkage. The average weld shrinkage measured was 1.5 mm, with a spread of 0.25 mm.

TABLE I
FRICTION MEASUREMENTS

Test	1	2	3	Avg.	μ
Aluminium on Vessel	23.5°	26°	24°	24.5°	0.456
Aluminium on Shim on Vessel	13°	14°	15°	14°	0.249
Shim on Vessel	13.5°			13.5°	0.24
Aluminium on Shim	25°			25°	0.466

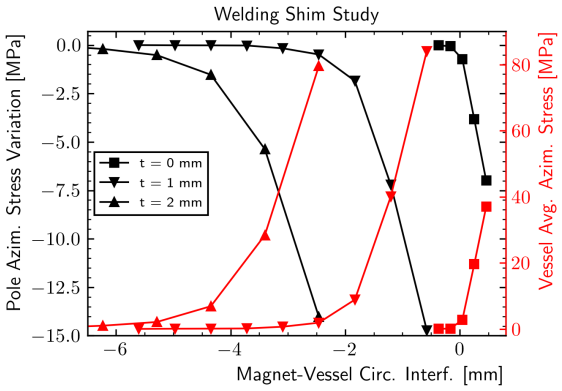

Fig. 3. Pole and vessel stresses after welding at room temperature, as a function of the circular interference and the welding shim thickness.

B. Total Variation

The recently built MQXFA01 cold mass was welded with the 'traditional' procedure (no welding shim). The SS shells were machined to a developed length determined using the measured average magnet aluminum cylinder circumference value and the average weld shrinkage value. After the two half SS shells were placed onto the magnet and they were tack welded, the obtained cold mass shell outer diameter was measured at several locations. After the weld was completed, the cold mass outer diameter was measured again and compared with the magnet circumference measurements performed before shell installation. Summing all the effects, the final variation of the circular interference is within ±0.6 mm: this value can be used as a reference for the error on the circumferential interference.

C. Magnet/Vessel Friction Coefficient Measurement

Sliding tests were performed to verify the friction coefficient between the aluminum shell of the MQXFA Magnet, the vessel and the shims. The results are reported in Table I. In the test with aluminium, shims and vessel, the shims slid on the vessel. The tests suggest that the friction coefficient between steel and aluminium components is equal to 0.45, and steel to steel equal to 0.24.

V. FE Modeling of the Welding Shim

A 2D FE model of the MQXF magnet was used to test the impact of the welding shim on the magnet performances. A deformed shape of the magnet after welding, with the welding shim installed, is shown in Fig. 1. The circular interference is introduced as an offset in the contact elements gap. The welding shim is introduced as an additional offset.

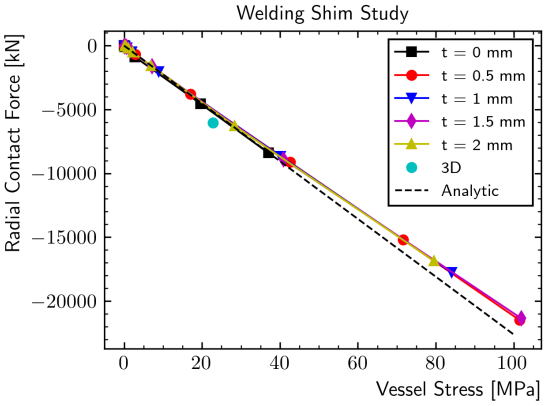

Fig. 4. Radial force between the vessel and the aluminum shell as a function of the circumferential interference. The force does not depend on the welding shim thickness.

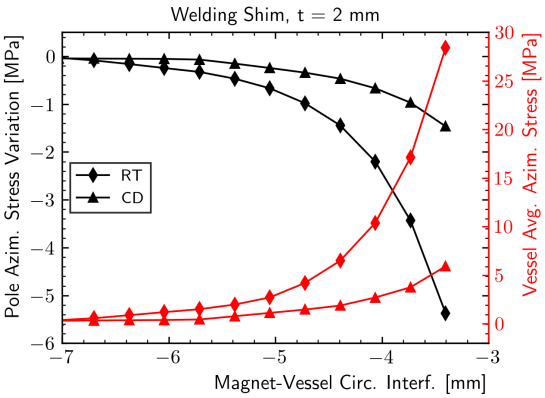

Fig. 5. Pole and vessel stress variation as a function of the circumferential interference, at room temperature and after cooldown. The differential thermal contraction results in a loss of interference.

The simulation follows the magnet assembly and consists of the following steps: magnet loading, welding with the shim, cooldown, powering, thermal cycling. Only the results after welding and cooldown are shown hereafter, as the model showed that the welding shim does not have an impact on the magnet in the following steps, as desired.

A. Room Temperature Results

The results of the FE model after welding at room temperature are shown in Fig. 3. The plot shows the remarkable difference in the impact of circular interference variations on the pole and vessel stresses. In particular, it can be seen that the welding shims allow for the desired buffer region, where the increase in stress is very gradual: with no shim (t = 0 mm), increasing the interference of 1 mm gives an increase of pole azimuthal stress of 15 MPa; with a 2 mm shim, the same increase can be as low as 1 MPa. In other words, we can conclude that the welding shim achieves its purpose of lowering the sensitivity to the circumferential interference tolerances. Obviously, this is true only in the regions of low vessel stress, since when the vessel gets in complete contact

TABLE II
MAIN WELDING SHIM PARAMETERS FOR THE MQXF MAGNET

		Room Temperature				Cryogenic Temperature			
	Interf.	σ_{pole}	σ_{vessel}	F_r	η_f	σ_{pole}	σ_{vessel}	F_r	η_f
	mm	MPa	MPa	kN	/	MPa	MPa	kN	/
Target	-4.52	-1.3	5.7	1440	4.8	-0.2	1.7	450	3.3
Target - 0.6 mm	-5.12	-0.6	2.6	640	2.1	-0.4	1.1	207	1.5
Target + 0.6 mm	-3.92	-2.8	13.2	3300	11.0	-0.8	3.2	870	6.3
Lower Limit	-5.4	-0.2	2.0	470	1.6	-0.5	0.8	138	1.0
Higher Limit	-3.8	-3.2	15.5	3535	11.8	-0.9	3.5	872	6.3

with the shim and the magnet, the slope is similar to the one with no shim installed.

The radial contact force is a function only of the vessel stress, and can be computed with the first part of Eq. 1. The model results, shown in Fig. 4, confirm this. The longitudinal contact force available before the magnet slips with respect to the vessel is then simply the radial contact force times the friction coefficient, equal to 0.45 (see Section IV-C).

B. Cryogenic Temperature Results

During cooldown, the contact condition between the magnet and the vessel changes because of their different thermal contraction: the (computed) integral magnet thermal contraction is equal to 3.54 mm/m, while the stainless steel is equal to 2.95 mm/m [13]. This results in a loss of stress both on the vessel and on the pole, as shown in Fig. 5 for the 2 mm thick shim case. As a consequence, to return to the same stress (and force) level, an increase in circular interference of 1.2 mm is needed.

C. Design Target

The magnet to vessel interference can be chosen on the basis of the acting loads, and the allowable stress increase in the winding pole. A safety factor η_F is defined as the ratio between the computed contact force and the required force. A target shim thickness of 2 mm was considered. The FE results are reported in Fig. 6 considering the force safety factor against the transportation loads at room temperature (top), and against the quench pressure wave (bottom). The design aims for a minimum safety factor of 1.5 on the available longitudinal force both at room temperature and at cold. Even if the quench load is lower, it requires higher interference: this effect is due to the loss of contact force during cooldown. Because of the tolerances, this safety factor has to be achieved at the design target -0.6 mm (see IV-B). This means that, on average, the safety factor applied to the produced cold masses will actually be higher. Table II reports the main results as a function of the applied interference, considering the design target, the minimum and maximum value of the interference, and the lower and higher limit cases obtained respectively with a force safety factor of 1, and a pole stress variation of 3.2 MPa.

VI. CONCLUSION

We have proposed a novel design that can improve the control on the amount of the contact forces between the stainless steel vessel and the magnet. This design is particularly

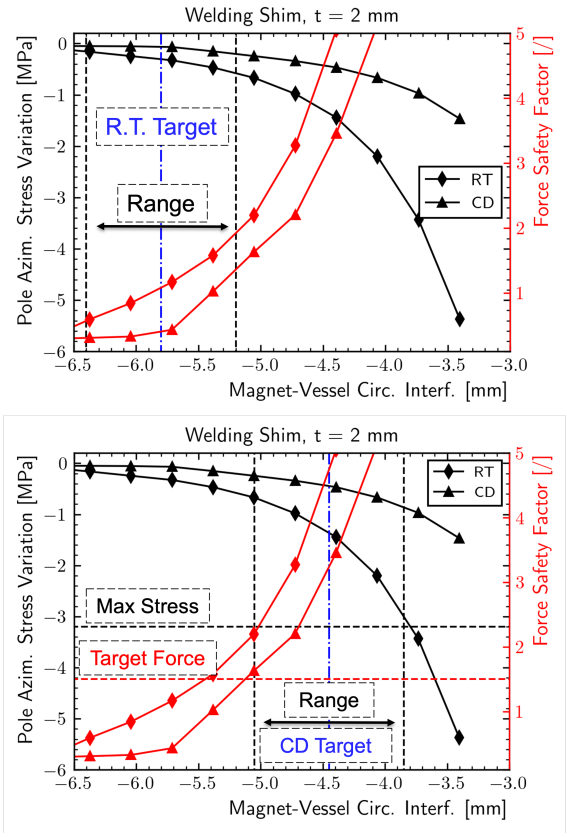

Fig. 6. Target results at Room Temperature (RT) and after cooldown (CD), considering the expected variation of the interference, the safety factor on the longitudinal loads, and the pole stress variation at warm (top), and at cold (bottom).

useful in those cases where a minimum contact force between the vessel and the magnet is required. The numerical models demonstrate that the shim allows for a lower sensitivity to the tolerances on the magnet to vessel circumferential interference. This effect grows with the shim thickness, introducing an easy way to compensate for eventual variations in magnet size or vessel developed length.

The design was numerically tested on the MQXFA magnet, where it allows the prevention of relative motions between the vessel and the magnet, with minimal impact on the coil stress increase. The target design proposes a 2 mm thick shim, which would give an increase in pole stress at room temperature of 1.3 MPa, and a total force at room temperature of 1440 kN and 450 kN after cooldown. This provides a safety factor on the required forces of 4.8 and 3.3 respectively.

REFERENCES

[1] P. F. Dahl *et al.*, "Superconducting magnet models for ISABELLE," *IEEE Transactions on Nuclear Science*, vol. 20, no. 3, pp. 688–692, 1973.

[2] M. Anerella *et al.*, "The RHIC magnet system," en, *Nuclear Instruments and Methods in Physics Research Section A: Accelerators, Spectrometers, Detectors and Associated Equipment*, The Relativistic Heavy Ion Collider Project: RHIC and its Detectors, vol. 499, no. 2, pp. 280–315, 2003.

[3] L. Rossi, "The LHC main dipoles and quadrupoles toward series production," *IEEE Transactions on Applied Superconductivity*, vol. 13, no. 2, pp. 1221–1228, 2003.

[4] M. Karppinen *et al.*, "Design of 11 T twin-aperture Nb_3Sn dipole demonstrator magnet for LHC upgrades," *IEEE Transactions on Applied Superconductivity*, vol. 22, no. 3, pp. 4 901 504–4 901 504, 2012.

[5] S. I. Bermudez *et al.*, "Mechanical analysis of the Nb_3Sn 11 T dipole short models for the high luminosity lhc," *Superconductor Science and Technology*, 2019.

[6] H. Kaiser, "Design of superconducting dipole for HERA," en, p. 4,

[7] J. Strait *et al.*, "Tests of full scale SSC R&D dipole magnets," *IEEE Transactions on Magnetics*, vol. 25, no. 2, pp. 1455–1458, 1989.

[8] S. Caspi *et al.*, "The use of pressurized bladders for stress control of superconducting magnets," *IEEE Transactions on Applied Superconductivity*, vol. 11, no. 1 II, pp. 2272–2275, 2001.

[9] P. Ferracin *et al.*, "The HL-LHC low-β quadrupole magnet MQXF: From short models to long prototypes," *IEEE Transactions on Applied Superconductivity*, 2019.

[10] P. Ferracin *et al.*, "Development of MQXF: The Nb_3Sn low-β quadrupole for the HiLumi LHC," *IEEE Transactions on Applied Superconductivity*, vol. 26, no. 4, pp. 1–7, 2016.

[11] L. Rossi and O. Brüning, "High Luminosity Large Hadron Collider a description for the european strategy preparatory group," no. 284404, 2012.

[12] G. Vallone *et al.*, "Mechanical performance of short models for MQXF, the Nb_3Sn low-β quadrupole for the HiLumi LHC," *IEEE Transactions on Applied Superconductivity*, pp. 1–1, 2016.

[13] R. J. Corruccini and J. J. Gniewek, "Thermal expansion of technical solids at low temperatures; a compilation from the literature," en, National Bureau of Standards, Gaithersburg, MD, Tech. Rep. NBS MONO 29, 1961, NBS MONO 29.